Contemporary Physics, 1994, volume 35, number 5, pages 329–346

Nuclear structure

P. E. HODGSON

Our current ideas about nuclear structure are reviewed with particular reference to recent developments. Exotic nuclei far from the valley of stability are now being studied, as well as high-spin states of deformed nuclei. The limitations of the shell model are reviewed, with the effects due to short-range correlations between nucleons given special attention. Nucleons in the nucleus tend to group themselves into clusters, and this too affects nuclear structure.

1. Introduction

In 1912, Rutherford discovered the structure of the atom, showing that it is composed of a central nucleus surrounded by electrons. It was very natural for him to probe deeper and to try to find the structure of the nucleus. Throughout the 1920s and 1930s he devised experiments to reveal this structure. He discussed the problem with Bohr, who told him that he was wasting his time, because according to his ideas about quantum mechanics the nucleus is just a structureless soup that occasionally emits particles; it is therefore meaningless to ask about nuclear structure. Discouraged by this, Rutherford abandoned his search (Wilson 1983)†. With hindsight the apparatus available to him was not sufficiently sensitive for his purpose, but the story is a striking illustration of the debilitating effects of the Copenhagen interpretation of quantum mechanics; it prevents us from asking perfectly reasonable questions and thus discourages innovative research.

After the war, many experiments showed increasing evidence that nuclei have a shell structure, similar to that in atoms. The principal difference is that, whereas the electrons in the atom move in the field of the nucleus, the nucleons in the nucleus move in the field generated by all the other nucleons. The shell model has proved astonishingly successful in accounting for a range of nuclear properties in a very simple way.

Nuclei are composed of neutrons and protons, collectively referred to as nucleons. Each nucleus is thus specified by the number N of neutrons and the number Z of protons, which together give the mass number $A = N + Z$. All nuclei can therefore conveniently be represented by squares on the N–Z plane, as shown in figure 1. Some nuclei are stable and others unstable, and these are distinguished by different colours. It is notable that the stable nuclei lie on a banana-shaped band centred on $N = Z$ for light nuclei and curving away to $N > Z$ for heavier nuclei. This curve is the result of two opposing tendencies: nuclei with $N = Z$ are particularly stable but the electrostatic or Coulomb repulsion of the protons tends to destabilize heavy nuclei with large Z and thus favours nuclei with a neutron excess.

Many experiments showed that nuclei with N or Z equal to one of the magic numbers 8, 20, 28, 50, 82 and 126 have greater stability than their neighbours and provided evidence for the nuclear shell model. It was found by Mayer and Jensen that these numbers may be obtained by assuming that the nucleons move independently in a one-body potential with a spin–orbit term, as described in section 2. This model does not, however, take account of the effects of short-range correlations between nuclei, which are discussed in section 3.

Recent experimental advances have made it possible to produce and study nuclei far from the stability line, and these exotic nuclei provide a useful testing ground for theories of nuclear structure. Such nuclei are described in section 4.

According to the shell model, completed shells of nucleons are stable spherical structures with the nucleons coupled together in pairs so that the total angular momentum is zero. The properties of the nucleus, and in particular its angular momentum and its low-lying excited states, are then determined by the couplings of the nucleons outside the inert core. It was soon found, however, that this fails to account for the large quadrupole moments of many nuclei, and in 1950 Rainwater suggested that the extra nucleons can polarize the core so that it becomes spheroidal. Some nuclei

Author's address: Nuclear Physics Laboratory, Department of Physics, University of Oxford, Keble Road, Oxford OX1 3RH, UK.

†Astonishingly, Wilson adds that Bohr's view of the nucleus as an unstructured soup of particles 'is the view still accepted by modern physicists'.

0010-7514/94 $10.00

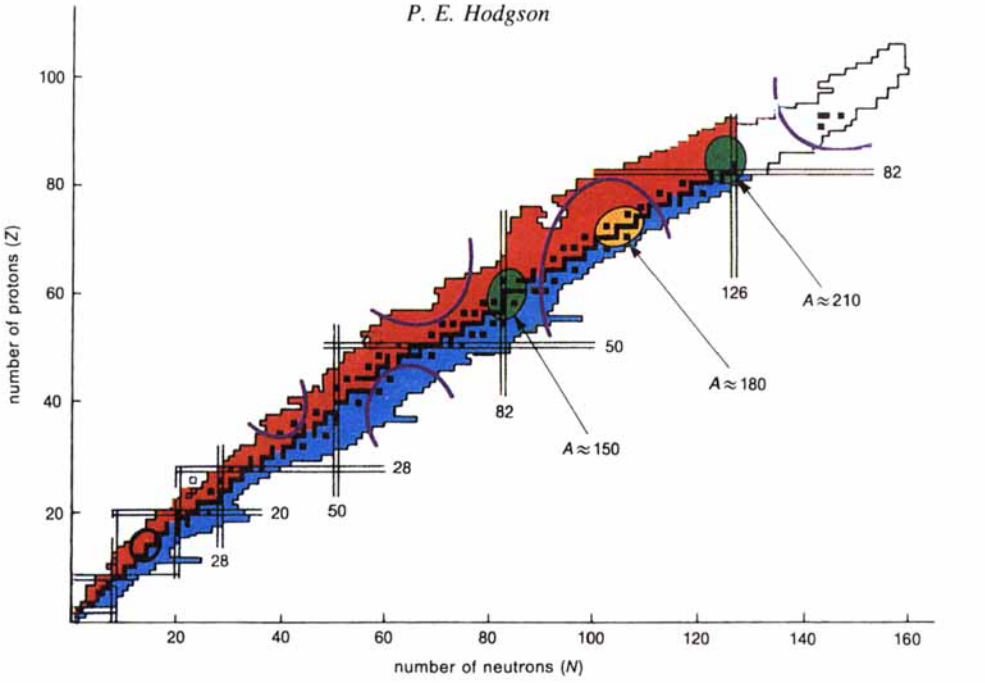

Figure 1. Nuclear chart showing the naturally occurring nuclei in black, the proton-rich nuclei in red and the neutron-rich in blue. The mass number A is the sum of the number (N) of neutrons and the number (Z) of protons, and the horizontal and vertical lines show the magic numbers. The regions of large deformation are away from the magic numbers and are shown in purple. The most favoured regions for high-spin isomers (discussed in section 5) are shown in green for the spherical and non-spherical spin traps and in orange for the prolate K traps (Walker and Dracoulis 1994).

are therefore deformed even in their ground state, and they can rotate if they receive additional energy. It is also possible for the whole cloud of nucleons to vibrate; so we can think about these nuclei in terms of changes in shape. A detailed theory of nuclear deformations was subsequently developed by Aage Bohr and Ben Mottelson, and in recent years the study of highly excited nuclei in heavy-ion reactions has led to many new discoveries such as superdeformation, hyperdeformation and spin traps as described in section 5. The nucleons inside the nucleus can coalesce into clusters, and the cluster structure of nuclei is described in section 6.

Since nuclei are made up of nucleons, it should be possible to calculate the structure of nuclei from a knowledge of the nucleon–nucleon interaction. This interaction is known in considerable detail from studies of proton–proton and proton–neutron scattering and from the properties of the deuteron. Unfortunately, however, attempts to do this failed. It is not even possible to calculate accurately the binding energy of the triton, the simplest nucleus after the deuteron. This could be due to inadequacies in our knowledge of the nucleon–nucleon interaction, but it is more likely that there are additional forces that act only when three nucleons are present. In any case, the mathematical difficulties of this approach become insuperable when the numbers of nucleons become large.

Even though nuclei are inherently very complicated, their properties and behaviour are in some respects quite simple, and this suggests that they may have a simple explanation. To explore this we use models, that is we make simple assumptions about nuclear structure that can be formulated mathematically and enable us to calculate nuclear properties that can be compared with experiment.

All our measurements of nuclear structure are made by recording individual events, such as the emission of a γ-ray or the inelastic scattering of a proton. Our theories of nuclear structure and reactions, however, give only the probability distributions, such as the half-life or the differential cross-section corresponding to these individual events. Quantum mechanics, by its very nature, enables us to calculate only the average behaviour of a large number or ensemble of similar systems. All our sophisticated nuclear theories are quantum mechanical, and so we can analyse only the average properties of nuclei. As Einstein believed, quantum mechanics is not the final theory, and it may well be that a more detailed deterministic theory will ultimately be found. So, while at present we have to calculate quantum-mechanically, we can still think about the behaviour of individual nucleons in the nucleus and their relations with each other. This is done, for example, by Anagnastatos in the work described in section 2. This may well stimulate new lines of thought and new experiments that could lead the way to a detailed microscopic theory of nuclear structure (Brody 1993).

It is helpful to think of nuclei in a simple way as a number of nucleons interacting with each other and moving around in a small approximately spherical region. Their time-

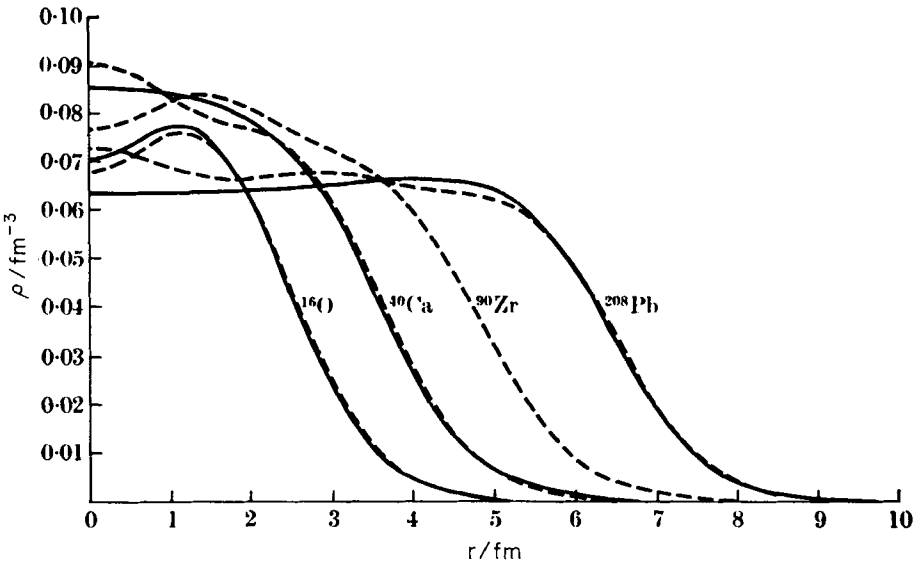

Figure 2. Nuclear charge distributions determined by electron scattering (—) and by mean-field calculations (---). These distributions are approximately uniform in the nuclear interior and fall off quite rapidly in the surface region (Negele 1970).

averaged positions can be expressed as proton and neutron density distributions. Since these nucleons have a finite size and repel each other at small distances, their density distributions are approximately uniform inside the nucleus and, since they attract each other strongly at larger distances, the density falls rapidly on the outside, giving a well defined surface as shown in figure 2. An exception to this is provided by some nuclei that are nearly unstable to neutron emission which have a neutron halo extending to large distances; such exotic nuclei are considered in section 4. The neutron–proton interaction is stronger than that between like nucleons, and this tends to lock the neutron and proton distributions together, making the spatial extent of the neutron and proton distributions very similar. Each nucleon moves on a well defined orbit in the mean field generated by the other nucleons and has a definite energy and the quantum numbers associated with the orbit. Each orbit has its own density distribution. Occasionally two nucleons collide and interact strongly, changing their trajectories. Sometimes two protons and two neutrons combine to form an α-particle, and this also moves in a quantum orbit until it is broken up by a further collision.

The structure of the nucleus is dynamic, and not static like a crystal. It may, however, be the case that the average positions of the nucleons, the spatial density distributions, have regions of higher probability that show a regular structure. This has been studied using the isomorphic shell model, which is able to account for many nuclear properties.

Over the years, many models of nuclei have been developed, each aimed at furthering our understanding of some particular properties. The models are formulated mathematically and, as the formalism proliferates, it is easy to lose sight of the nucleus itself. Inevitably, the models have their limitations, for they can each only give us knowledge of a part of the complicated reality. Nevertheless it is instructive to try to put these models together to improve our knowledge of nuclear structure as a whole. This is the main object of the present review, so emphasis will be laid on the visualizable semiclassical aspects of nuclei. For completeness several well known theories are described briefly, but more attention is given to recent and lesser-known results. These show clearly that there is still much that is to be learned about nuclear structure.

In a brief review it is possible to mention only a few topics, with illustrative examples. Inevitably many important papers receive no mention, and several highly interesting subjects, such as those concerning the mesonic and hyperonic degrees of freedom of nuclei, are omitted.

2. Shell structure

Many features of nuclear structure can be very simply understood by assuming that all the nucleons move independently in a mean field. We thus replace the action of all the other nucleons on a particular nucleon by a one-body potential. This can be calculated with difficulty and some approximations from the nucleon–nucleon interaction, but it is much simpler to assume that it is given by the phenomenological potential

$$V(r) = V_c(r) + Uf(r) + U_s g(r)\mathbf{L}\cdot\boldsymbol{\sigma}, \qquad (1)$$

where $V_c(r)$ is the electrostatic potential, and U and U_s are the strengths of the central and spin–orbit potentials. The radial dependence $f(r)$ follows rather closely the nuclear density distribution, conveniently parametrized by the Saxon–Woods form factor $f(r) = \{1 + \exp[(r - R)/a]\}^{-1}$, where $R = 1{\cdot}25A^{1/3}$ fm is the radius parameter and $a = 0{\cdot}65$ fm is the surface diffuseness parameter, which

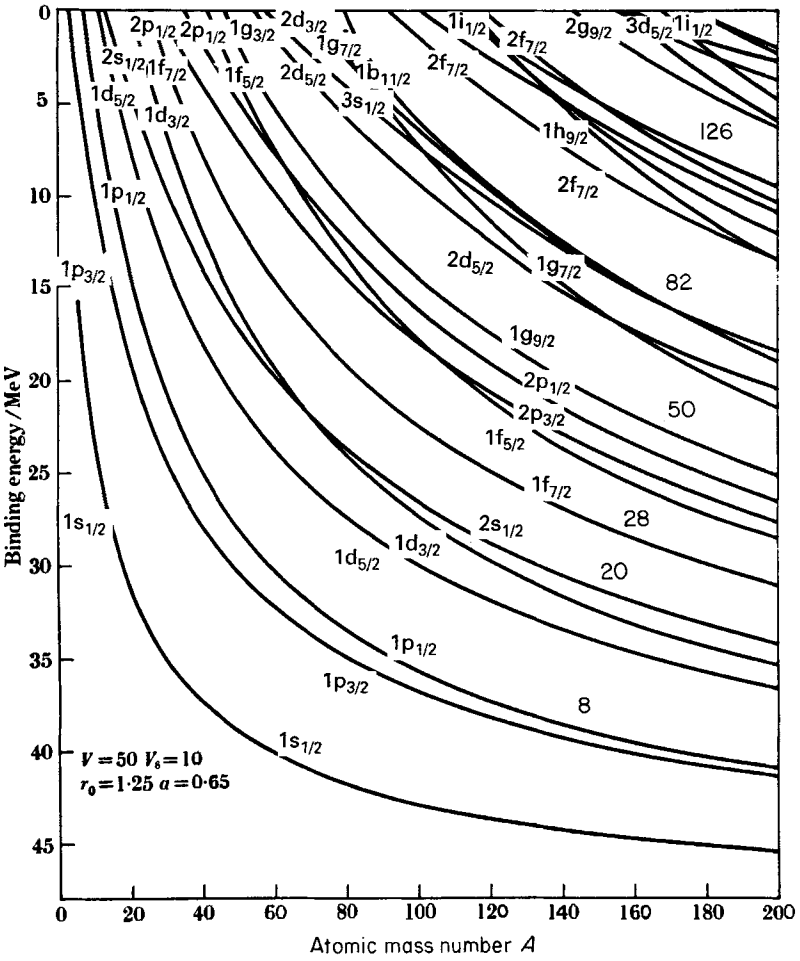

Figure 3. Neutron single-particle states in a Saxon–Woods potential as a function of A. The states form shells, and the total numbers of nucleons for completed shells give the magic numbers (Hodgson 1971).

governs the rate of fall-off in the surface region. The radial variation of the spin–orbit term has the form $(\mathrm{d}f(r)/\mathrm{d}r)/r$, which is peaked on the nuclear surface.

This potential has a series of discrete eigenstates characterized by their energies and quantum numbers. If we allow nucleons to occupy these states, starting from the lowest and restricting the number of nucleons in each state by the Pauli principle, we obtain a useful model of nuclear structure. With potential depths $U = 50$ MeV and $U_s = 14$ MeV, the energies of the states correspond well to those found experimentally using one-nucleon transfer reactions. These states are shown in figure 3 as a function of atomic number.

The nuclear density distributions can be calculated from this model by squaring and adding the wavefunctions of all the nucleons. The charge distributions found in this way are in excellent agreement with those found from analyses of electron elastic scattering at high energies, and the matter distributions with those found similarly from analyses of proton elastic scattering (Ray and Hodgson 1979, Malaguti *et al.* 1982).

This potential can also account for unbound states in the continuum with the addition of an imaginary potential to give the widths of the states. This is the optical potential that describes the scattering of nucleons by nuclei (Hodgson 1963, 1971, 1994). The strengths of the real, imaginary and spin–orbit potentials depend on energy in a smooth way, so that the nucleon mean field is able to unify bound and scattering states (Hodgson 1990). A further unification of the real and imaginary parts of the potentials can be obtained using dispersion relations which connect them together (Hodgson 1992).

This model of nuclear structure is most useful for nuclei in their ground states. It can account for some low-lying excitations by promoting nucleons to unoccupied states, but this soon becomes unreliable particularly if there are several nucleons outside closed shells; their angular momenta couple together in different ways and the model provides no way of calculating the energies of the resulting states.

The simple shell model can be developed in a more fundamental and self-consistent way following a theory originally developed by Hartree for atoms. If the nucleon density distribution and the nucleon–nucleon interaction are known, the potential at any point can be calculated. With this potential, the Schrödinger equation can be solved to give the

wavefunctions of all the particles, and hence an improved nucleon density distribution. This calculation can be iterated until it converges, that is the potential calculated from a particular distribution of particles gives that same distribution, so that a self-consistent field has been found. This calculation is much more difficult for nuclei than for atoms because there is no dominant central field and the nucleon–nucleon interaction is more complicated and less well known than the Coulomb potential. The method was developed by Fock to take account of the antisymmetrization required by the Pauli principle, and the equations with fully antisymmetrized wavefunctions are called the Hartree–Fock equations.

Instead of using the nucleon–nucleon interaction it is possible to use an effective interaction with parameters adjusted to fit selected data. To simplify the calculation, it is usual to assume that completed shells are inert, and to include only the orbits of the nucleons outside the core in the iteration.

Over the years, many Hartree–Fock calculations of increasing sophistication have been made, and it remains one of the most powerful methods of calculating the ground-state properties of nuclei. Like the simple shell model, however, it is not suitable for calculating the properties of excited states.

A more sophisticated shell model can be constructed by calculating the wavefunctions Ψ_i for a complete set of nuclear states and then diagonalizing the matrix

$$<\Psi_i|H|\Psi_j> \tag{2}$$

where H is the nuclear Hamiltonian. However, the number of nuclear states is unlimited and we do not know the nuclear Hamiltonian; so once again we have to use a simple model.

If we assume that the nucleons move independently, the Hamiltonian is the sum of their potential and kinetic energy operators

$$H = \sum_{i=1}^{A}\left(-\frac{\hbar^2}{2m}\nabla_i^2\right) + \sum_{i>j}^{A} V(r_{ij}), \tag{3}$$

where $V(r_{ij})$ is the potential between the ith and jth nucleon and r_{ij} is the distance between them. This omits three-body forces, although the failure to calculate the binding energy of the triton with two-body forces alone suggests that they are not negligible. In shell-model calculations it is hoped that the main effects of any three-body forces will be represented by effective two-body forces.

We now use the result of the simple shell model, namely that the effects of all the two-body interactions between nucleons can be quite well represented by a central one-body potential $V(r)$ acting on each nucleon independently. Adding and subtracting the sum of these potentials, the Hamiltonian then becomes

$$H = \sum_{i=1}^{A}\left(-\frac{\hbar^2}{2m}\nabla_i^2 + V(r_i)\right) + \left(\sum_{i>j}^{A} V(r_{ij}) - \sum_{i=1}^{A} V(r_i)\right), \tag{4}$$

which may be written

$$H = H^0 + H^1, \tag{5}$$

where H^0 is the Hamiltonian of the simple shell model and H^1 a perturbing Hamiltonian.

We now use the simple shell model to generate a limited set of wavefunctions, parametrize the perturbing Hamiltonian H^1 and perform the matrix diagonalization. The parameters of H^1 are fixed to give the energies of a few low-flying excited states, and then the model can be tested by seeing how well it gives the energies of the higher states. Since the wavefunctions of states of different angular momenta J are orthogonal, the calculation is performed separately for each J.

The difficulty with this apparently simple calculation is that many nucleon states or orbitals must be included to obtain a realistic result, and then the number of nuclear states increases rapidly. This remains true even if completed shells are considered to be inert and are excluded from the analysis. For example, with six identical nucleons populating the $1d_{5/2}$, $2s_{1/2}$ and $1d_{3/2}$ orbitals above an inert core there are 12 states for each nucleon (including magnetic orbitals) and thus 924 nuclear states. Recognizing the distinction between neutrons and protons increases this to 853,576 nuclear states. Thus even quite simple cases lead to impracticably large matrices. Nevertheless, many ingenious methods of improving the calculations have been made and used to analyse a wide range of nuclei (Mayer and Jensen 1955, De Shalit and Feshbach 1974, Brussaard and Glaudemans 1977, Lawson 1980, Talmi 1993).

These calculations can be improved by using more realistic forms for the nuclear Hamiltonian and using a larger set of basis states. It is generally found that the improvements in the fits to the data are rather marginal, and that the optimized form of the perturbing Hamiltonian is specific to a particular nucleus, whereas ideally one would like to have a form applicable to a wide range of nuclei.

Another type of shell-model calculation considers in a unified way all the nuclei in a particular region of the periodic table and uses as parameters not those of the interaction potential but the matrix elements themselves. The same matrix elements enter into the calculation of the energy levels in different nuclei and into the calculation of all observables corresponding to one- and two-body operators. The number of states increases much more rapidly than the number of two-body matrix elements and so a large number of observables are determined by a much smaller number of matrix elements. Since the shell-model Hamiltonian contains only one- and two-body operators, it is completely defined by the matrix elements of these operators in the chosen set of basis states. They are thus treated as adjustable parameters whose values are determined by comparison with selected experimental data. These values are then used to calculate a much wider set of nuclear properties, and comparison with

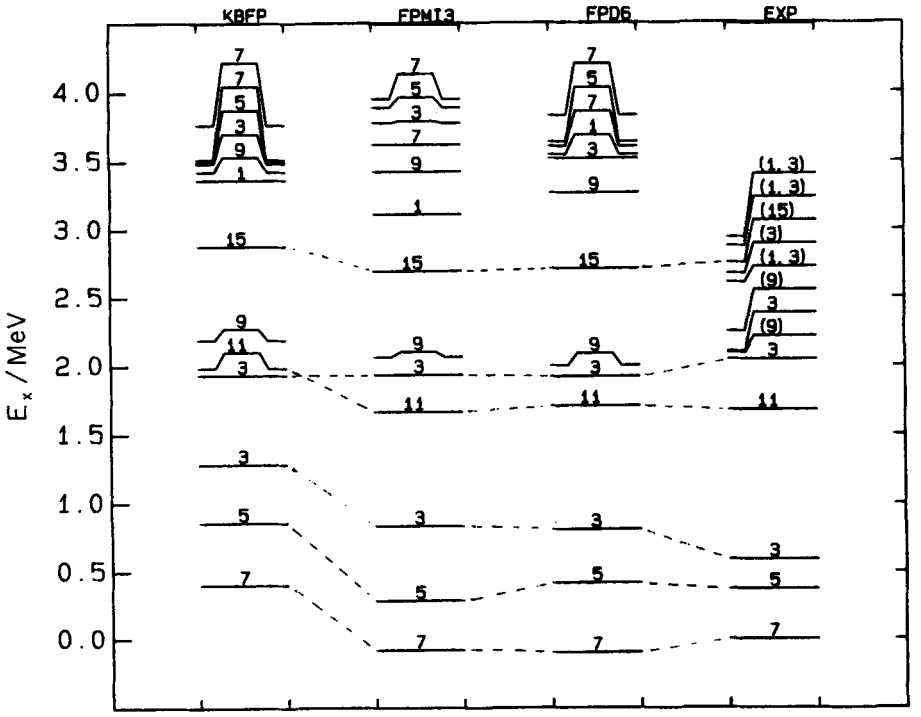

Figure 4. Comparison of theoretical and experimental energy spectra for low-lying natural-parity levels in fp-shell nuclei. This diagram is for ^{43}Ca ($T = 3/2$) and the number on each state is $2J$. The experimental ground-state energy is taken as zero. The ground-state energies shown for three different interactions labelled FPD6, FPM13 and KBFP have been calculated relative to ^{40}Ca. The spectra are complete up to the highest level shown unless stated otherwise. Uncertain spin and parity assignments are indicated in parentheses. Observed levels of indefinite spin and parity are omitted from the experimental spectrum (Richter *et al.* 1991).

the measured values enables the validity of the model to be assessed.

Many of these shell-model calculations have been made for lighter nuclei, using various approximations and truncations of the model space. In a recent analysis by Richter *et al.* (1991) of 1f2p shell nuclei it was found possible to fit the energies of low-lying states with a r.m.s. deviation of 178 keV. Their fit to states in ^{43}Ca is shown in figure 4. It is also possible to calculate many other nuclear properties, including the ground-state magnetic dipole and electric quadrupole moments and some of these are compared with the experimental values in tables 1 and 2.

These calculations can also be applied to heavier nuclei near closed shells, but away from closed shells they soon become impracticable owing to the large number of valence nucleons. For such nuclei the collective models described in section 5 may be used, or a simpler version of the shell model which will now be described.

Although the nucleons in the nucleus are constantly in motion, the mean-field theories of nuclear structure show regions of higher density characteristic of a static structure. Thus Hartree–Fock calculations of the density distribution of ^{12}C show three regions of higher density at the vertices of an equilateral triangle corresponding to the three α-particles postulated in the α-particle model of that nucleus (Eichler and Faessler 1970). Similar calculations of the structure of ^{24}Mg by Rae (1988) show the structure of the ground and several excited states of that nucleus as different spatial arrangements of α clusters.

This aspect of nuclear structure has been studied semiclassically on the nucleon level by Anagnostatos (1985) who has

Table 1. Ground-state magnetic dipole moments μ compared with the shell-model calculations of Richter *et al.* (1991). T is the isospin of the ground state.

Nuclide	$2J$	$2T$	μ_{exp}/μ_n	μ_{th}/μ_n
^{41}Ca	7	1	−1·594 780(9)	−1·913
^{41}Sc	7	1	5·43(2)	5·793
^{43}Ca	7	3	−1·3174(2)	−1·754
^{43}Sc	7	1	4·62(4)	4·547
^{44}Sc	4	2	2·56(3)	2·218
^{45}Ca	7	5	−1·3278(9)	−1·663
^{45}Sc	7	3	4·7567(2)	4·753
^{45}Ti	7	1	(−)0·095(2)2	−0·354
^{47}Ca	7	7	−1·380(24)	−1·585

Table 2. Ground-state electric quadrupole moments Q compared with shell-model calculations of Richter *et al.* (1991).

Nuclide	$2J$	$2T$	Q_{exp}/electrons fm^2	Q_{th}/electrons fm^2
^{41}Ca	7	1	−6·2(12)	−7·3
^{43}Ca	7	3	−4·0(8)	−3·0
^{43}Sc	7	1	−26(6)	−20·0
^{44}Sc	4	2	10(5)	10·1
^{45}Ca	7	5	4·3(9)	3·1
^{45}Sc	7	3	−22(1)	−23·6
^{45}Ti	7	1	(−)1·5(15)	−11·5

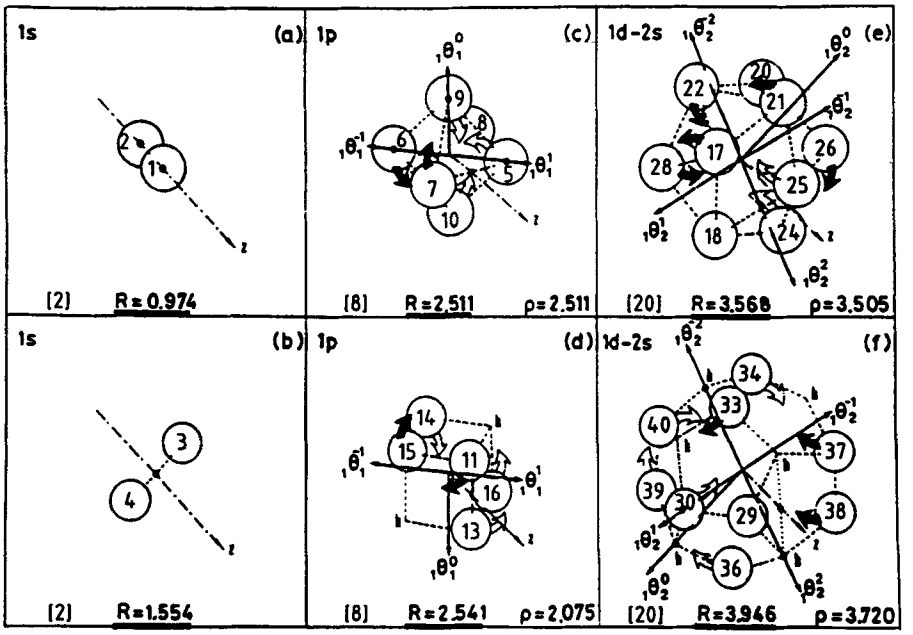

Figure 5. The isomorphic shell model for the nuclei up to $N = 20$ and $Z = 20$. The high-symmetry polyhedra in the upper row (i.e. the zerohedron, the octahedron and the icosahedron) stand for the average forms for neutrons (*a*) the 1s, (*c*) the 1p and (*e*) the 1d2s shells, while the high-symmetry polyhedra in the lower row (i.e. the zerohedron, the hexahedron (cube) and the dodecahedron) stand for the average forms of (*b*) the 1s, (*d*) the 1p and (*f*) the 1s2s shells for protons. The vertices of polyhedra stand for the average positions of nucleons in definite quantum states (τ, n, l, m, s). The letters h stand for the empty vertices (holes). The z axis is common for all polyhedra when these are superimposed with a common centre and with relative orientations as shown. At the bottom of each block the radius R (fm) of the sphere exscribed to the relevant polyhedron and the radius ρ (fm) of the relevant classical orbit equal to the maximum distance of the vertex state (τ, n, l, m, s) from the axis ${}_n\theta_l^m$ precisely representing the orbital angular momentum axis with definite n, l and m values are given. Curved arrows are shown to help the reader to visualize for each nucleon the axis round which it rotates where solid (open) arrows show rotations directed up (down) the plane of the paper. All polyhedra vertices are numbered as shown. The back (hidden) vertices of the polyhedra and the related numbers are not shown in the figure (Anagnostatos 1993).

developed the isomorphic shell model that combines shell- and cluster-model concepts. In this model the nucleons in each shell are in dynamic equilibrium and their average positions correspond to the Leech (1957) polyhedra (figure 5) for the spatial distribution of particles on a spherical surface. The particles occupy the vertices of the polyhedra and, in each shell, neutrons and protons occupy reciprocal polyhedra. The neutrons are assigned to the stable equilbrium polyhedra and the protons to the unstable equilibrium polyhedra and together these polyhedra are stable.

The neutrons and protons are treated as hard spheres of radii $r_n = 0{\cdot}974$ fm, and $r_p = 0{\cdot}860$ fm; these are the only parameters of the model and are very similar to the radii of nucleon bags in the quark model. The dimensions of the shells are then determined by the close packing of the shells.

The assignment of nucleons to the vertices of polyhedra follows the principles that identical particles on a shell are interchangeable and that for each particle position there is a symmetric counterpart. The total energy of the system is minimized, and this sometimes requires that particular symmetrically distributed vertices are left unoccupied. The structure of nuclei up to $N = Z = 20$ is shown in figure 5.

The cumulative numbers of neutrons or protons give the magic numbers, as shown in table 3. It is notable that these are obtained without introducing the concept of spin–orbit coupling. This suggests that the magic numbers are the result of very general symmetry considerations that can be represented in the shell model by introducing spin–orbit coupling (Anagnostatos 1985). The same magic numbers are predicted for clusters of two kinds of alkali atom (Anagnostatos 1988).

There is a one-to-one correspondence between the positions of occupied vertices and the sets of quantum numbers of the nucleon wavefunctions. The wavefunction of

Table 3. The isomorphic shell model (Anagnostatos 1985).

Neutrons					Protons				
	Vertices	Holes	$N=V-H$	ΣN		Vertices	Holes	$N=V-H$	ΣN
Zerohedron	2	0	2	2	Zerohedron	2	0	2	2
Octahedron	6	0	6	8	Hexahedron	8	2	6	8
Icosahedron	12	0	12	20	Dodecahedron	20	8	12	20
Icosidodecahedron	30	0	30	50	Hexahedron	8	0	8	28
Hexahedron	8	0	8	58	Icosahedron	12	0	12	40
Dodecahedron	20	8	12	70	Dodecahedron	20	8	12	52
Icosahedron	12	0	12	82	Icosidodecahedron	30	0	30	82
Hexahedron	8	0	8	90					
Rhombicosidodecahedron	60	24	36	126					

each nucleon is calculated from a harmonic oscillator potential with frequency

$$\hbar\omega = \frac{\hbar^2}{m<r^2>}(N+3/2), \tag{6}$$

where N is the harmonic oscillator quantum number and $<r^2>^{1/2}$ is the average radius of the shell.

Using the wavefunctions, the nuclear charge and matter distributions can be calculated together with the corresponding r.m.s. radii. The charge radii are more accurately known experimentally and these are given usually to better than 1% throughout the periodic table. A particularly severe test is provided by the relative radii through an isotopic sequence, and the result for the calcium isotopes is shown in figure 6. The calculated matter radius of the exotic nucleus ^{11}Li (see section 4) is 3·13 fm, in agreement with the experimental value. Nuclear charge distributions have also been calculated, and that for ^{16}O is in excellent agreement with experiment (Anagnostatos 1985).

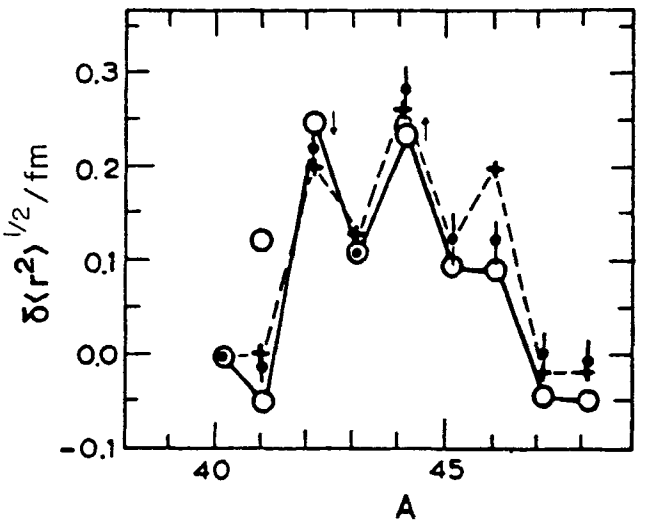

Figure 6. The relative r.m.s. charge radii of the calcium isotopes (Anagnostatos *et al.* 1991): (●), the experimental values; (○), (—), results of isomorphic model calculations; (---), calculations of Talmi (1984).

The angular momentum quantization axes are identically described by the rotational symmetries of the polyhedra. Thus these axes form, with respect to the common z axis of the polyhedra (taken as the quantization axis), the angles (Landau and Lifshitz 1962)

$$\theta_{nlm} = \cos^{-1}\left(\frac{m}{(l(l+1))^{1/2}}\right) \tag{7}$$

(Anagnostatos 1978, 1980a,b, Panos and Anagnostatos 1982). The directions of some of these axes are shown in figure 5.

The nucleon–nucleon potential is approximated by the difference between the two Yukawa potentials, and this allows the nuclear binding energies to be calculated. Most of these agree with the experimental values to within 1 or 2 MeV (Anagnostatos 1992).

The nuclei with nucleons outside the closed shells are no longer spherically symmetric and so have a quadrupole moment. The isomorphic shell model has been applied to calculate the quadrupole moments of 15 nuclei in the sd shell and the values obtained are in excellent agreement with experiment (Anagnostatos 1977).

For a harmonic oscillator potential, Ehrenfest's theorem shows that the average of the force over the wavefunction is equal to the classical force acting on the centre of the wavefunction. The isomorphic shell model can therefore be combined with the classical equations of motion to give a semiclassical simulation of nuclear structure (Anagnostatos and Panos 1990). In this model, the nucleons are given initial positions and velocities corresponding to the isomorphic shell model, so that their configurations have the normal density distribution, include short-range correlations and have the correct saturation properties (Anagnostatos and Panos, 1984, Anagnostatos 1985, 1989, Panos and Anagnostatos 1982). The subsequent motion of the nucleons is followed using the classical equations of motion with the internucleon potential given by the difference between the two Yukawa potentials.

Calculations for ^{16}O show that the radius of the matter distribution fluctuates about a mean value close to the experimental value of 2·65 fm. Similarly the mean nucleon

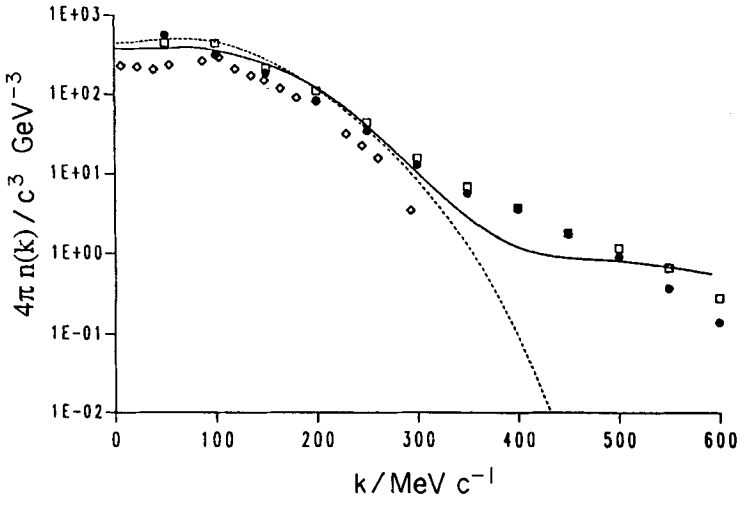

Figure 7. Nucleon momentum distribution in ^{12}C compared with calculations using the Hartree–Fock mean-field theory (. . .) and a theory that includes short-range correlations (—) (Ciofi degli Atti *et al.* 1989).

potential energies fluctuate, but their sum remains constant at 7·74 MeV per nucleon, compared with the experimental value of 7·89 MeV nucleon. This model of the nucleus is also useful for analysing heavy-ion collisions at high energies.

This work of Anagnostatos has succeeded in accounting for many detailed nuclear structure properties and deserves to be tested in more detail, both experimentally and theoretically.

3. Nucleon correlations in nuclei

The nucleons in the nucleus are incessantly moving; so we can ask what is their momentum distribution. This is known in several ways. The cross-sections of (p, 2p) and (e, e^{1}p) reactions, for example, in which an incident proton or electron knocks out a proton in the nucleus, depends on the magnitude and direction of the struck nucleon. Pion production in similar circumstances also depends on the internal momentum distribution; indeed it was first observed at incident energies lower than expected because sometimes the incident proton encounters a nucleon in the nucleus moving towards it with a high momentum.

Since the nucleon wavefunctions in momentum and coordinate space are Fourier transforms of each other, it might be thought easy to calculate the nucleon momentum distribution from the spatial distribution. This is not so; as shown in figure 7 the calculated momentum distribution is markedly below the measured distribution at high momenta. High momenta probe short distances; the source of the discrepancy at high momenta is the correlations among the nucleons of short range, which are not described by the independent particle model that is used to obtain the wavefunctions. The correlations depend on the nucleon–nucleon interaction, which is repulsive at very short distances and attractive at somewhat larger distances. When the nucleons collide, they are for a short time in a deep attractive potential with a hard-core repulsion at short distances and momentarily have high momenta. It is thus not possible to describe the spatial and momentum distributions of nucleons in the nucleus simultaneously by an independent particle model. It might be asked why these nucleons with very high momenta do not escape from the nucleus. The reason is that they are in a deep potential so that, although they have a high kinetic energy, their total energy is always less than the escape value.

The effect of the short-range correlations on the motions of the nucleons can be shown by considering the classical trajectories of the nucleons. Most of the time the nucleons move in the mean field and the trajectories are smoothly varying functions of position. Occasionally, however, they experience a close encounter with another nucleon and are sharply accelerated and deflected. The smooth parts of the trajectory correspond to the motion in the mean field and the abrupt changes to the short-range correlations with other nucleons that give rise to the high-momentum components in the nucleon momentum distribution. The difference between the trajectories with and without the short-range correlations is shown in figure 8.

The effect of the short-range correlations on the trajectories shows the difficulty of determining the high-momentum components of the nucleon momentum distribution. If this is done by measuring the momenta of the two outgoing protons in a (p, 2p) reaction in which an incoming proton knocks another proton out of the nucleus, the momentum of the struck nucleon is determined by assuming that the reaction is essentially a two-body collision inside the nucleus. The effect of the other nucleons is assumed to be small and can be allowed for by assuming that the collision takes place in a nuclear medium with a complex refractive index. This model of the (p, 2p) reaction is good for the smooth parts of the trajectories where the influence of the other nucleons is indeed small, and so the low-momentum part of the nucleon momentum distribution below the Fermi energy is well determined. However, the model breaks down in the region

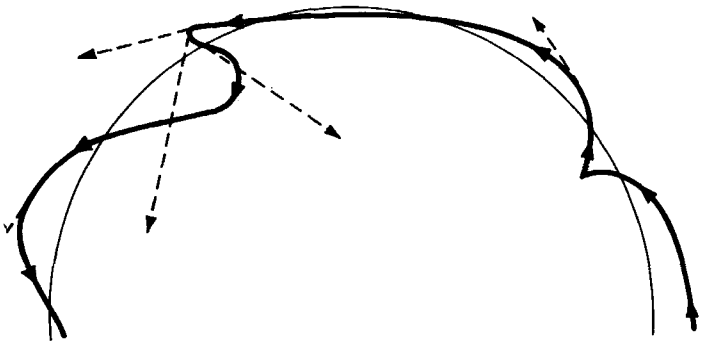

Figure 8. The classical trajectory of a nucleon in a nucleus. The heavy line shows the actual trajectory; and the light line the trajectory given by the single-particle mean-field model. The dotted arrows show the instantaneous nucleon velocities (Gottfried 1963).

of the kinks in the trajectory because there is another nucleon present, and it is precisely these parts of the trajectory that correspond to the high-momentum components. Thus, although we know that there are high-momentum components in the nucleon momentum distribution, it is very difficult to determine them precisely (Gottfried, 1963).

In order to calculate the effects of short-range nucleon–nucleon correlations in the nucleus, it is necessary to use theories that go beyond the mean-field theory. Such theories define a correlation operator that transforms the wavefunction $\Phi(\mathbf{r}_1, \mathbf{r}_2, \ldots, \mathbf{r}_A)$ of the uncorrelated many-body shell-model wavefunction into that of the correlated system $\Psi(\mathbf{r}_1, \mathbf{r}_2, \ldots, \mathbf{r}_A)$. There are several ways of doing this, and among them the simplest to visualize is that of Jastrow (see Antonov *et al.* (1993, chapters 3 and 4)). This method takes into account the short-range repulsion or hard core in the nucleon–nucleon interaction that prevents the nucleons coming closer than the hard-core radius r_c. This is done by introducing factors $f(r_{ij})$ that extinguish the wavefunction for all r_{ij} less than the core radius r_c, so that

$$\Psi(\mathbf{r}_1, \mathbf{r}_2, \ldots, \mathbf{r}_A) = N \prod_{1 \leq i < j \leq A} f(r_{ij}) \Phi(\mathbf{r}_1, \mathbf{r}_2, \ldots, \mathbf{r}_A) \tag{8}$$

where Φ is a Slater determinant of single-particle wavefunctions and N is the normalization constant. The correlation functions is defined to be zero for $|\mathbf{r}_i - \mathbf{r}_j| \leq r_c$ and to be $1 - \exp(-\beta|\mathbf{r}_i - \mathbf{r}_j|^2)$ otherwise. The value of the correlation range β and of the other parameters are determined by minimizing the energy of the correlated system.

The main effect of imposing the nucleon–nucleon correlations is to enhance the high-momentum components of the nucleon momentum distribution, as shown in figure 7. By calculating the mean-field potentials that give the correlated wavefunctions directly, it is found that the short-range correlations have a rather small effect on the potentials and wavefunctions corresponding to the filled states, as shown in figures 9 and 10. The short-range correlations mainly affect the motion of the nucleons above the Fermi energy; this is important for the analysis of stripping reactions that populate such states.

4. *Exotic nuclei*

Recent advances in experimental techniques have made it possible to produce beams of nuclei far from the valley of greatest stability. This is usually done by spallation reactions in which an incident heavy ion strikes a target of a heavy nucleus. Both nuclei are shattered, and the fragments are analysed by a mass spectrograph into beams of nuclei of different mass and change. By judicious choice of the interacting nuclei, different regions of the periodic table can be favoured, and beams of particular nuclei isolated.

Since heavy nuclei are neutron rich, this method tends to produce more neutron-rich fragments, and in this way several

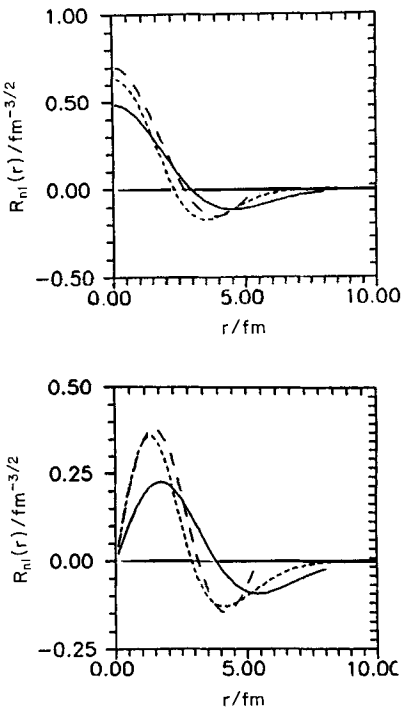

Figure 9. Single-particle wavefunctions for (*a*) the 2s and (*b*) the 2p states of ^{40}Ca (Antonov *et al.* 1994): (---), correlated orbitals calculated by the coherent density fluctuation model; (— —), shell model wavefunctions corresponding to a square-well potential with infinite walls; (—), shell model wavefunctions in a harmonic oscillator potential.

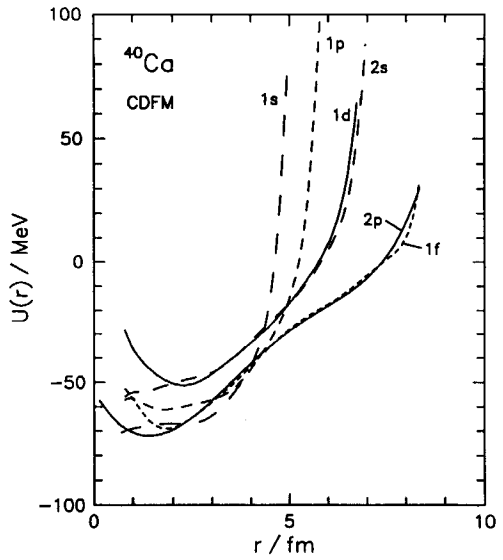

Figure 10. Effective potentials for ^{40}Ca showing the difference between those of filled states (1s, 1p, 1d and 2s) and those of unfilled states (2p and 1f) due to the short-range correlations (Antonov *et al.* 1994).

exotic nuclei such as ^{6}He, ^{11}Li, ^{11}Be, ^{14}Be and ^{17}B have been studied (Zhukov *et al.* 1993). Such nuclei have a central core of normal density surrounded by an extended halo that consists of the excess neutrons. Thus ^{6}He is an α-particle with two halo neutrons (Danilin *et al.* 1991, Ferreira *et al.* 1993) and ^{11}Li has a ^{9}Li core also with two halo neutrons. This has been shown by studies of the transverse momentum distribution of ^{9}Li fragments from the reaction ^{11}Li + C (Kobayashi *et al.* 1988) and by optical model analyses of the quasi-electric scattering of ^{11}Li by ^{12}C (Thompson *et al.* 1993). It is only just bound, by 0·2 MeV, whereas ^{10}Li is unbound by 0·8 MeV. In general, such nuclei near the stability limit have an even number of neutrons whereas neighbouring nuclei with an odd number of neutrons are unbound, whatever the number of protons. The radii of these nuclei can be determined from the total interaction cross-section, and some results are shown in figure 11(*a*): those of the exotic nuclei are anomalously high, owing to the extended halo. Irradiation by γ-rays excites the giant dipole resonance which is split into two states: one corresponding to the core neutrons and protons oscillating against each other and the other, of much lower energy, due to the halo neutrons oscillating against the core nucleons, as shown in figure 11(*b*). This latter excitation is called the soft giant dipole resonance, and its presence has been confirmed by studies of the transverse momentum distribution from ^{11}Li fragmentation (Zhukov *et al.* 1994).

Many attempts have been made to calculate the structure of the exotic nuclei using cluster models, Hartree–Fock Faddeev and shell-model calculations (Thompson *et al.* 1993). It has proved very difficult to account for all the measured characteristics, particularly to bind ^{11}Li while leaving ^{10}Li unbound. A recent calculation by Gómez *et al.* (1992) has solved most of these problems. They began with a Hartree–Fock calculation using a force proposed by Skyrme, which is known to give a good overall description of the bulk properties of nuclei. The resulting wavefunctions were then used in a shell-model calculation that gave the ground-state energies, the core and two-neutron separation energies, the density distribution and other nuclear properties. Their results for the energies of many light nuclei are shown in figure 12, and it is notable that ^{11}Li is bound and ^{10}Li is unbound. The one- and two-neutron separation energies are given quite well and also the radii, except that the value for ^{11}Li is less than the observed value. This can,

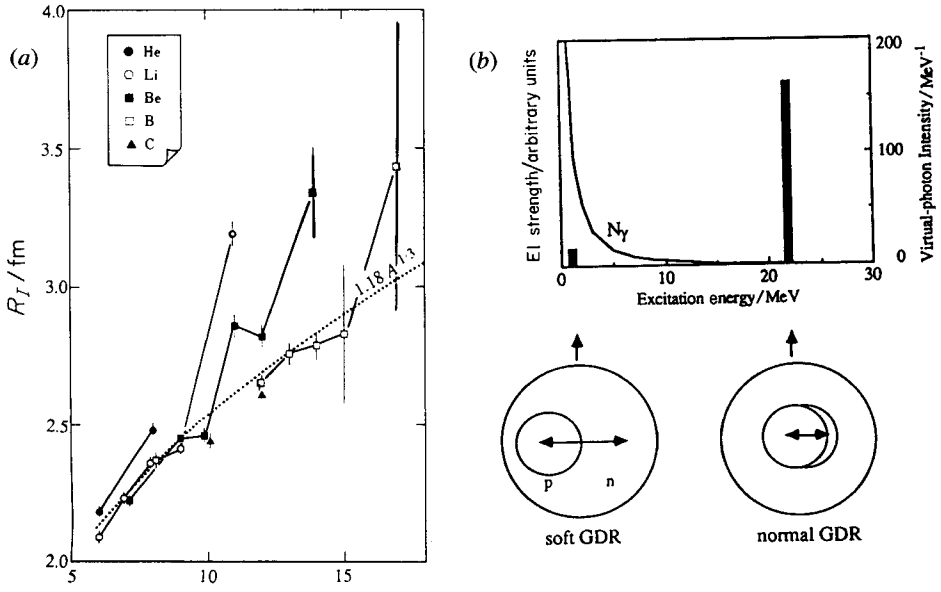

Figure 11. (*a*) Interaction radii for a range of light nuclei showing the very high values characteristic of halo nuclei. The curve gives the radius $1.12A^{1/3}$ characteristic of nuclei across the periodic table (Tanihata 1988). (*b*) Schematic picture of the soft and the normal giant dipole resonance (GDR) in ^{11}Li. The E1 strengths of both resonances are shown together with the virtual photon spectrum seen by a ^{11}Li projectile on a lead target at 0·8 GeV per nucleon (Kobayashi *et al.* 1989).

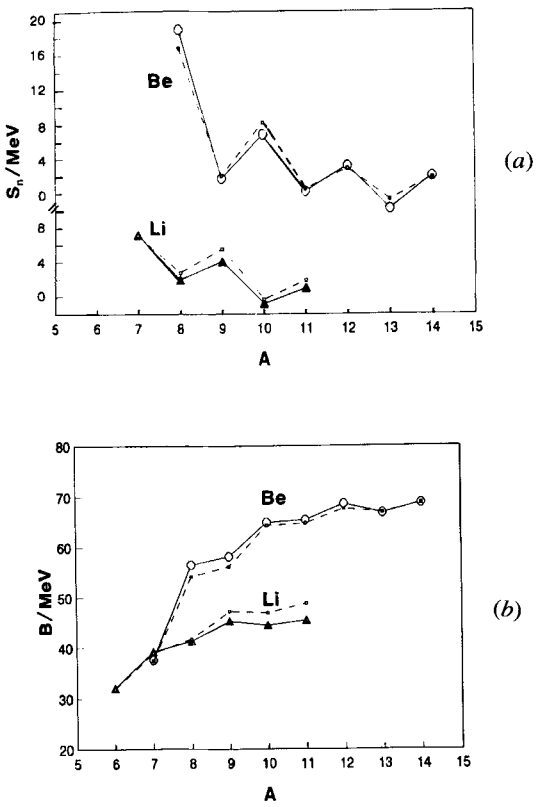

Figure 12. (*a*) Binding energy of lithium and beryllium isotopes: (---), calculated values; (●), experimental beryllium values; (▲), experimental lithium values. (*b*) Neutron separation energy of lithium and beryllium isotopes: (---), calculated values; (▲), experimental lithium isotope values; (●), experimental beryllium isotope values. (Gómez, Prieto and Poves, 1992).

however, be rectified by slightly modifying the parameters of the Skyrme force.

5. Collective excitations

Some nuclei are deformed in their ground states and can be excited into rotational motion, retaining their shapes. Others are spherical in their ground states and can be excited into vibrational motion. At high excitation energies, rotational nuclei can change from oblate (pancake) to prolate (cigar), and some show the extreme deformation known as superdeformation, a prolate deformation with a ratio of major to minor axis of two (Hodgson 1987).

These overall shapes of rotating nuclei are mainly governed by classical forces, and it is found that the curves of energy as a function of angular velocity for different shapes cross each other. At low angular velocities, oblate shapes are energetically favoured, like the Earth, while at high angular velocities a prolate shape is favoured. Unlike classical bodies, however, excited nuclei exist in discrete states, and the correlated motions of the individual nucleons determine their detailed structure.

In contrast with single-particle excitations, the nucleons move collectively in such excitations. The excited states form rotational or vibrational bands and de-excitation usually takes place by γ emission by successive transitions down a band. Collective nuclei often have many bands based on states of different structure, and transitions can take place, usually with more difficulty, from one band to another.

A rotational band may be identified using the quantum-mechanical expression for the energy of a rotator:

$$E_J = \frac{\hbar^2}{2\mathscr{I}} J(J+1) \tag{9}$$

where $\mathscr{I}$ is the moment of inertia and J the total angular momentum quantum number. A rotator with ground state 0^+ has a series of states forming a band with $J = 0, 2, 4, \ldots$ and energies given by equation (9). The values of J increase by two because all states must have the same parity $\pi = (-)^J$. The moment $\mathscr{I}$ of inertia can be determined from equation (9) and is usually found to be about a third or half the classical rigid-body value, indicating that the nucleons in the spherical core do not participate in the rotation.

Heavy nuclei in the regions away from the magic numbers (see figure 1) can be excited to highly excited states by heavy-ion reactions. An off-centre collision between nuclei, for example ^{40}Ca on ^{112}Sn, is the only way to give high angular momentum to the compound system without immediately breaking it up. Studies of the γ-rays emitted from such highly excited nuclei have revealed complicated structures of bands and, about ten years ago, Twin *et al.*

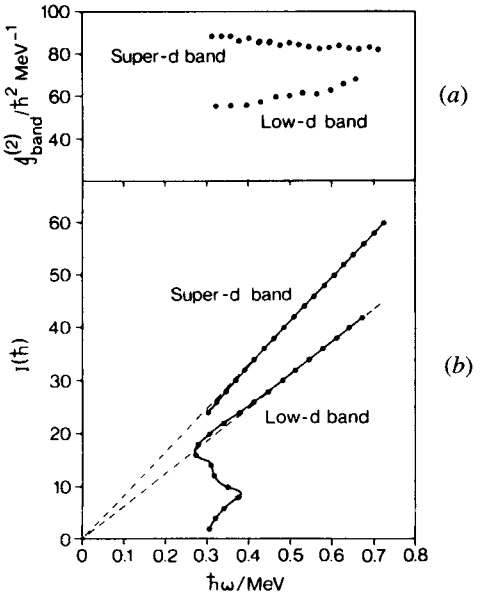

Figure 13. (*a*) Moment of inertia as a function of energy for the superdeformed band and for a lower-energy deformed band in ^{152}Dy. (*b*) Angular momentum as a function of energy for the same two bands. The linear relation corresponds to equation (9) (Twin *et al.* 1986).

(1983) found evidence for bands with very high moments of inertia. Analysis of such a superdeformed band in ^{152}Dy indicated a prolate shape with an axis ratio of 2 to 1. Such superdeformed shapes are in accord with theoretical calculations and have now been found in several other nuclei. The moment of inertia is very constant along the superdeformed band, indicating a very rigid shape. As shown in figure 13, it is more rigid in the superdeformed band than in bands of lower energy.

It can happen that there is such a large difference between the structure of a state and the states of lower energy that it is very difficult for it to decay and so it has a long life. Long-lived excited states of nuclei have been known since their discovery by Otto Hahn in 1921, and they are called isomeric states or isomers. What is new is the discovery of isomers of very high spin. In 1962 an isomer of ^{212}Pu was found with a half-life of 45 s and a spin of about $18\hbar$, which decays almost entirely by α emission because γ emission is hindered by a large spin difference between the state itself and states of lower energy. This is called a spin (or yrast) trap (Walker and Dracoulis 1994).

The structure of this nucleus is shown in figure 14(*a*); two neutrons and two protons orbit in the same direction around the spherical ^{208}Pb core. This state has a high spin because the spins of the four nucleons add together, and also a low energy due to its high symmetry. There are therefore no states of similar spin and lower energy to which it can decay; so all that can happen is for the four nucleons to escape together as an α-particle. Another spin trap was found in ^{212}Fr by Byrne *et al.* (1990). This trap has an excitation energy of 8·5 MeV a spin of $34\hbar$ and a lifetime of 24 μs and decays by an E3 transition.

More recently, a long-lived trap of spin $16\hbar$ at 2·4 MeV has been found in ^{178}Hf, with a half-life of 31 years. There are no states of $15\hbar$ or $14\hbar$ at lower energies and so its γ decay must be at least $3\hbar$, corresponding to an E3 transition with a half-life of about 0·1 s. This is very long on the nuclear time scale, but still far short of the observed value of about 10^9 s. The difference is due to a change in the symmetry of the nucleus in going from the $16\hbar$ to the $13\hbar$ state. The projection of the angular momentum vector on the symmetry axis of the nucleus is a conserved quantum number K, and this has to change from 16 to 8. Thus to conserve K the γ-ray quantum number must change by eight units. This is almost impossible, but it is found that the rotation breaks the symmetry of the paired nucleon orbits, thus facilitating the transition. The transition rate does, however, drop by a factor of about 100 for each unit of K, so allowing for the three units taken by the E3 transition gives the required factor of 10^{10}. This isomer is thus both a spin and a K trap.

Spin traps are most likely to be found among heavy nuclei, for then the individual nucleons have a high spin. A few of these spins coupled together then give a high-spin state. To eliminate the possibility that the remaining nucleons provide a lower state of high spin to which the isomer could decay, they should all be paired, preferably as a magic or doubly magic nuclei, as in ^{212}Po. This indicates the green regions of the periodic table with $A \approx 150$ and $A \approx 210$ in figure 1 for spin traps. There is a limit of about $30\hbar$ to the spin because too many nucleons outside the core can cause it to become unstable.

A K trap requires a strongly deformed core and so suitable nuclei are expected in the regions far away from closed shells. Together with the requirement of a heavy stable nucleus, there is only one region of the periodic table where such nuclei are expected namely the orange region around $A \approx 180$ in figure 1. The nucleus ^{178}Hf is in this region. Spin traps have recently been found in ^{176}Ta and ^{177}Ta (Dasgupta *et al.* 1994).

Even if you know where to look for them, spin and K traps are difficult to make. The favoured method is by a heavy-ion reaction, which forms a compound system with the required high angular momentum. The compound nuclei produced in this way usually have a large neutron excess, and these have to evaporate before the isomer is reached. This takes some time and in heavy nuclei it is very likely that fission occurs before the isomer is reached. Sometimes, as in ^{178}Hf, there

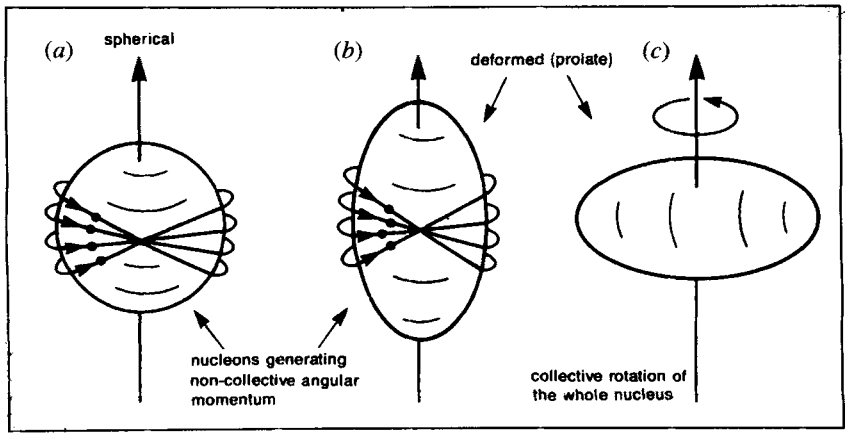

Figure 14. Nuclei can have high spin in several ways (Walker and Dracoulis 1994): (*a*) correlated nucleons rotating in the same direction around a spherical core; (*b*) the same around an axis and (*c*) the collective rotation of the whole nucleus perpendicular to the symmetry axis.

is no stable heavy-ion beam–target combination, and so neutron capture or α-particle bombardment has to be used instead.

These spin traps are far from being esoteric playthings of nuclear structure physicists. It is likely that our very existence depended on them, because the nuclear reactions in the stars far in the past that led to the formation of the heavy elements required isomers that live long enough to allow the capture of an additional proton or neutron. The other practical consequences of isomers may soon be important; in the design of fusion reactors, care has to be taken to avoid materials that could be transformed into isomers by intense radiation, because this could lead to an unacceptable build-up of radioactivity. This is particularly serious for ^{178}Hf, since its half-life of 31 years is neither so small that the radioactivity quickly decays nor so large that the amount actually decaying is small.

6. The cluster structure of nuclei

The emission of α-particles by nuclei was interpreted by Rutherford as evidence that the α-particle is to be regarded as an 'important secondary unit in the building up of the heavier nuclei and probably of nuclei in general' (Wilson 1983, p. 576). The nucleons in the nucleus can thus occasionally form transient substructures that persist until they are broken up by an encounter with another nucleon. Of all such substructures or clusters the α-particle is the most favoured because of its high symmetry and binding energy.

The α decay of nuclei was the first nuclear process studied quantum-mechanically, when Gamow proposed a simple model that was able to account for the vast range of measured half-lives. He proposed that α-particles exist inside the nucleus, and that they bounce backwards and forwards between the walls. Each time they hit the potential barrier there is a finite chance that they will overcome it and be emitted. This probability can be evaluated quantum-mechanically and is extremely sensitive to the width of the barrier. This model has proved very successful in accounting for the relative half-lives of α decay and in its latest versions for the absolute values also, to within an order of magnitude (Buck and Merchant 1989, Merchant *et al.* 1989, Merchant and Buck 1989, Buck *et al.* 1990, 1991a,b, 1992).

Accurate calculations of the α decay half-life proved very difficult, essentially because the individual nucleons comprising the α-particle must be described by the shell model, and then a very large basis is needed to describe them as they move away from the decaying nucleus. This difficulty has been overcome by Varga *et al.* (1992a,b) by adding a cluster model component to the shell-model wavefunction, so that the total wavefunction becomes

$$\Psi = \Psi(\text{shell}) + \Psi(\text{cluster}). \tag{10}$$

The cluster-model wavefunction is an antisymmetrized product of the intrinsic wavefunctions $\phi_c(\xi_c)$ and $\phi_\alpha(\xi_\alpha)$ of the core nucleus and the emitted α-particle respectively and the wavefunction $\phi(R)$ of their relative motion, where R is the separation of their centres of mass:

$$\Psi(\text{cluster}) = A[\Phi_c(\xi_c)\Phi_\alpha(\xi_\alpha)\phi(R)]. \tag{11}$$

The decay is described by a Gamow wavefunction, which at large α-core distances becomes an outgoing Coulomb wave, and the α-particle itself is described by 1 s harmonic oscillator wavefunctions.

The shell-model basis states are obtained by diagonalizing the Hamiltonian

$$H = \sum_{i=1}^{4}(T_i + U_i) + \sum_{i>j}^{4} V(i,j), \tag{12}$$

where T_i is the nucleon kinetic energy, U_i the average single-particle potential and $V(i,j)$ the residual interaction.

The calculation of the α decay width was carried out avoiding the approximations inherent in previous work, and all the parameters were fixed from independent experimental data. Thus the parameters of the single-particle and harmonic oscillator potentials were chosen to fit the experimental energies of the single-particle states and the binding energies of the initial and final nuclei.

This formalism was applied to calculate the absolute decay width of ^{212}Po, which decays to ^{208}Pb. This is a particularly favourable case, as the final nucleus has a double-closed shell. The decay width was calculated from the **R**-matrix formula

$$\Gamma = 2P_L \frac{\hbar^2}{2M_\alpha a_L} g_L^2(a_L), \tag{13}$$

where M_α is the reduced mass, P_L the Coulomb penetration factor, a_L the channel radius and $g_L(a_L)$ the clustering amplitude. The result $\Gamma = 1{\cdot}45 \times 10^{-15}$ MeV agrees well with the experimental value of $1{\cdot}5 \times 10^{-15}$ MeV. The α-particle occupancy of the state is about 20 times the best shell-model estimates, and the probability of formation of an α-particle inside the nucleus is 0·302.

A related aspect of α clustering in nuclei is the α-particle momentum distribution, and this has recently been calculated by Antonov *et al.* (1992). Knowledge of this momentum distribution is important for calculations of α-particle knock-out reactions. α clustering is to be expected on energy grounds, and it has been shown that a nucleon gas is likely to condense into α-particles if the density falls to a value about one third of that in the centre of the nucleus (Brink and Castro 1973).

A detailed study of the properties of α cluster matter has been made by Tohsaki-Suzuki (1989) using the generator coordinate method (GCM). He considered cubic lattices of α-particles in one, two and three dimensions with an effective

interaction proposed by Brink and Boecker. The nucleon spatial wavefunctions at $R_1, R_2, \ldots, R_n$ in GCM space are

$$\phi_i(r) = (\pi b^2)^{-3/4} \exp\left(-\frac{1}{2b^2}(r - R_i)^2\right), \quad (i = 1, 2, \ldots, N), \tag{14}$$

where b is the size parameter of the four-nucleon δ cluster.

The configuration of N α clusters is then given by a Slater determinant of the $4N$ nucleon wavefunctions characterized by the distance parameter s giving the separations of the α-particles in the lattice in the x, y and z directions. The microscopic Hamiltonian is expressed as the sum of kinetic and potential energy terms with direct and exchange components. The total energy per particle was then calculated as a function of the size parameter b and the distance parameter s. It was found that the energy rapidly converges to limiting values as the number of α-particles increases, and these limits, in one, two and three dimensions, characterize infinite α matter. For a three-dimensional lattice, the energy has a sharp minimum at $s = 2{\cdot}8$ fm but is relatively insensitive to the size parameter b with optimum value 1·3 fm. The minimum in the energy curve is not so sharp in one and two dimensions. The value of the binding energy per nucleon in three dimensions is 14·5 MeV, very similar to that in nuclear matter.

The concept of a mean field, so useful for nucleons in nuclei (see section 2) can also be applied to unify our knowledge of α-particle bound states and elastic scattering. The real part of the α-particle potential can be obtained by a double folding of the nuclear and α-particle densities with the nucleon–nucleon interaction, giving

$$V_\alpha(r) = \int\int \rho(r_1)\rho(r_2)v(|\mathbf{r} + \mathbf{r}_2 - \mathbf{r}_1|)\,\mathrm{d}\mathbf{r}_1\,\mathrm{d}\mathbf{r}_2. \tag{15}$$

A good approximation to the radial variation may be obtained by using a delta function for the nucleon–nucleon interaction and analytical expressions for the nuclear densities. For many purposes it is more convenient to use an analytic expression for the potential, such as the Saxon–Woods potential or the cosh potential (Buck and Merchant 1989, Buck *et al.* 1992):

$$V_\alpha(r) = \frac{V[1 + \cosh(R/a)]}{\cosh(r/a) + \cosh(R/a)}. \tag{16}$$

The energies, widths and B(E2) transition rates for the α-particle states in ^{16}O were successfully analyzed using an α–^{12}C folded potential obtained by Buck *et al.* (1975); subsequently they extended the analysis to ^{20}Ne, which has a pronounced α cluster structure (Katō and Bandō 1978, Chung *et al.* 1978). More recently, there has been much interest in applying the model to heavier nuclei, especially to the nuclei analogous to ^{16}O and ^{20}Ne in the fp shell, namely ^{40}Ca and ^{44}Ti.

The nucleus ^{44}Ti(= ^{40}Ca + α) is a particularly favourable case, and it has been extensively studied (Horiuchi 1985, Michel, Reidemeister and Ohkubo 1986a,b, 1988, Ohkubo 1988, Wada and Horiuchi 1988, Merchant *et al.* 1989). The earlier analyses were made of the cross-section of the ^{40}Ca(^{6}Li, d) reaction at 28 and 32 MeV (Fulbright *et al.* 1977) by applying the distorted-wave theory to determine the quantum numbers of many of the bound and unbound states of ^{44}Ti. As shown in figure 15, these states are quite well given by the α cluster model, using the α-particle optical potential that fits very well the extensive data on the elastic scattering of α-particles by ^{40}Ca (Delbar *et al.* 1978). It is notable that the model predicts a $N = 13$, $K = 0^-$ negative-parity band of α-particle states in ^{44}Ti, which at that time had not been observed. The 1^-, 3^- and 5^- members of this band were subsequently found by Yamaya *et al.* (1990) using an incident energy of 50 MeV (figure 16). This provides striking confirmation of the α cluster model.

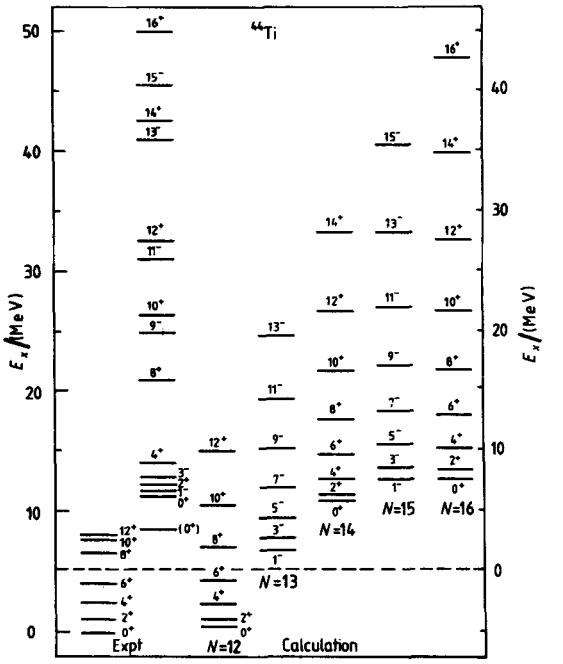

Figure 15. A comparison of the calculated energies of the bands with principal quantum numbers $N = 12$ to $N = 16$ of the α cluster states in ^{44}Ti generated by a finite-range folded potential with the experimental data, where the right-hand energy scale refers to the α + ^{40}Ca system (Merchant *et al.* 1989).

The absolute α-particle probabilities obtained in this work were, however, very low, ranging from 0·04 for the ground state to even lower values for the excited states. Such low values raised a serious question about the validity of the α cluster model. This was further investigated by Yamaya *et al.* (1993), who found that the spectroscopic factors are very sensitive to the values of the α-particle wavefunctions in the region of the nuclear surface. The previous analysis used a wavefunction obtained from a Saxon–Woods potential which was not obtained from α-particle elastic scattering, whereas

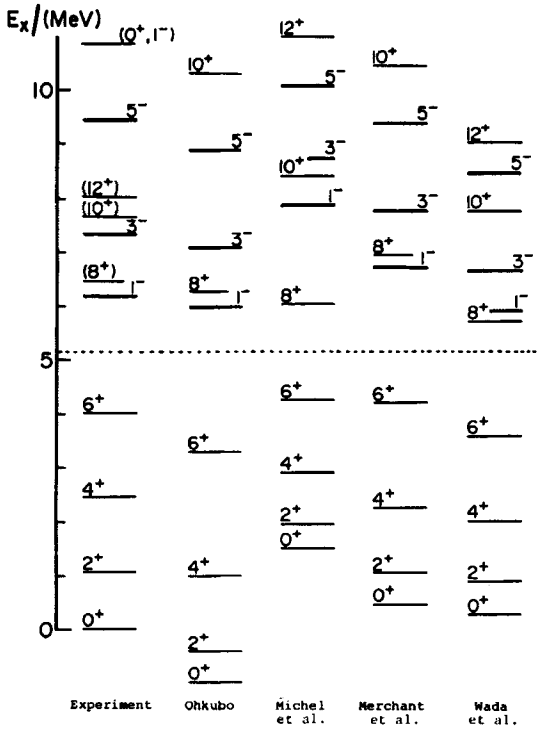

Figure 16. Observed parity doublet band in comparison with theoretical predictions of α cluster states in ^{44}Ti: (---), α-particle separation energy, the negative parity states observed by Yamaya *et al.* are clearly shown. The 10·86 MeV state is a candidate for the head of the higher nodal state of $N = 14$ or 15 (Yamaya *et al.* 1990).

later analyses such as that of Michel *et al.* (1986a, 1988) used the more realistic squared Saxon–Woods potential which gives smaller values of the wavefunction in the surface region, and hence larger spectroscopic factors between 0·1 and 0·2 for the $K = 0^+$ and $K = 0^-$ bands.

Many light nuclei, as mentioned in section 2, have a pronounced α-particle structure, and many aspects of their behaviour can be understood by considering them to consist of one or more α-particles interacting with each other and with the surrounding nucleons.

A particularly interesting class of α-particle states is provided by the α-chain states. These are usually excited states consisting of a linear chain of α-particles. Such states are more stable than might be thought because, in the case of ^{24}Mg for example, the energy of an oscillator quantum is about 24 MeV in a direction perpendicular to the chain but only about 4 MeV in the direction of the chain. It thus requires about 20 MeV to bend the chain.

The first of these is ^{8}Be, which has a well known rotational band consisting of 0^+, 2^+ and 4^+ states at 0, 3 and 11 MeV. The ground state is unstable by 92 keV, with a width of 6 eV, and the two higher states have widths of 1 and 3 MeV respectively. The next α-particle nucleus, ^{12}C has a 0_2^+ state at 7·65 MeV that is believed to have the structure of a linear chain of three α-particles (Brink 1966). This ^{12}C state preferentially breaks up into ^{8}Be + α and is known from elastic scattering to have a large charge radius.

There are no known 0^+ states of ^{16}O, that have ^{8}Be, ^{12}C(0_2^+) or four α-particles among their decay products. There are, however, three 2^+ states around 17 MeV that decay into ^{8}Be and at least one α-particle, and they may have a chain structure. There are several other possible candidates, and so chain states in ^{16}O may still be found. Calculations of α chain states in ^{12}C and ^{16}O have been made by Zamick and Zheng (1994).

In 1986, Marsh and Rae made calculations of the states of ^{24}Mg using a version of the Bloch–Brink cluster model and predicted a band of states around 45 MeV corresponding to a linear chain of six α-particles. Experimental evidence for this band has been found (Wuosmaa *et al.* 1992) at 48 MeV, approximately the energy predicted by Marsh and Rae. This state breaks up into two ^{12}C α chain states.

One of the remarkable features of the data of Wuosmaa *et al.* is that on resonance the cross-section has a very strong peak at 90° in the centre-of-mass system. Rae *et al.* (1992) found that this can be explained only if many partial waves contribute with particular relative phases. They suggest that the data are consistent with the resonance being due to an α-particle chain with a very large moment of inertia, so that the peak is due to the superposition of resonances that are essentially degenerate, their spacings being less than their widths. The angular distribution can thus be considered to be an approximate shape or angle eigenstate.

Rae and Merchant are able to account for the data in terms of α-particle resonances in a hyperdeformed potential. A semiclassical analysis gives the relatively small widths (Merchant and Rae 1994) and full quantum-mechanical calculations are also able to account for the observations.

Evidence for a state in ^{28}Si consisting of a chain of seven α-particles has been found (Rae and Merchant 1993, Simmons *et al.* 1993). The energy of this state is 60 MeV, within a few megaelectron volts of the predictions of Merchant and Rae (1992). Much work remains to be done to confirm the existence of α chain states.

Until quite recently it was thought that α-particles are the only nucleon clusters that can be emitted from nuclei. Then Rose and Jones (1984) found that, very rarely, ^{14}C nuclei can be emitted from ^{223}Ra, although α emission is far more likely. It was long known that such heavy-particle decays are energetically possible, but it was thought that the height of the Coulomb barrier made them essentially impossible. Subsequently, many other examples of heavy-particle radioactivity have been found (Price 1989). The decay rates can be calculated to better than an order of magnitude using the same simple barrier penetration model that was used for

α decay (Buck *et al.* 1994). Work is now in progress on the fine structure of these decays.

7. Conclusion

The nuclei of atoms provide a range of unique quantum systems of many strongly interacting particles that show many types of behaviour from single particle to collective. Although they are extremely complicated, nuclei have many simple features that may be described by models that give astonishingly accurate predictions. In this way, many aspects of nuclear structure are now well understood.

In recent years, however, the development of powerful new experimental techniques (in particular the 4π γ-ray detectors and the production of radioactive beams) have revealed a wealth of new phenomena that show unsuspected aspects of nuclear structure. Among these are the high-spin states corresponding to very deformed nuclei, the neutron haloes in light nuclei, the α-particle chain states and heavy-particle radioactivity.

The discovery of these remarkable phenomena shows the continuing vitality of nuclear structure physics and ensures that it will provide experimental and theoretical challenges for many years to come. Furthermore, it is finding increasing applications in astrophysics and reactor design.

Acknowledgements

I am grateful to Professor G. S. Anagnostatos, Professor A. N. Antonov, Professor R. C. Johnson, Dr B. R. Fulton, Dr A. C. Merchant and Dr I. Thompson and Dr P. M. Walker for valuable discussions and suggestions, and for sending copies of their papers, and to the authors of papers for permitting the figures to be included in this review.

References

Anagnostatos, G. S., Kosmas, T. S., Hefter, E. F., and Panos, C. N., 1991, *Can. J. Phys.*, **69**, 114.
Anagnostatus, G. S., 1977, *Atomkernenergie.* **29**, 207.
Anagnostatos, G. S., 1978, *Lett. Nuovo Cim.*, **22**, 507.
Anagnostatos, G. S., 1980a, *Lett. Nuovo Cim.*, **28**, 573.
Anagnostatos, G. S., 1980b, *Lett. Nuovo Cim.*, **29**, 188.
Anagnostatos, G. S., 1985, *Int. J. Theor. Phys.*, **24**, 579.
Anagnostatos, G. S., 1988, *Phys. Lett.* **A128**, 266.
Anagnostatos, G. S., 1989, *Phys. Rev.* C, **39**, 877.
Anagnostatos, G. S., 1992, *Can. J. Phys.*, **70**, 361.
Anagnostatue, G. S. 1993, Predeal Conference, Romania.
Anagnostatos, G. S., and Panos, C. N., 1990, *Phys. Rev.* **C42**, 961.
Anagnostatos, G. S., and Panos, C. N., 1984, *Lett. Nuovo Cim.*, **41**, 409.
Antonov, A. N., Hodgson, P. E., and Petkov, I. Zh., 1988, *Nucleon Momentum and Density Distributions in Nuclei* (Oxford: Clarendon Press).
Antonov, A. N., Hodgson, P. E., and Petkov, I. Zh., 1993, *Nucleon Correlations in Nuclei* (Berlin: Springer).
Antonov, A. N., Kadrev, D. N., and Hodgson, P. E., 1994, *Phys. Rev.* **C50**, 164.
Antonov, A. N., Nikolov, E. N., Petkov, I. Zh., Hodgson, P. E., and Lalazissis, G. A., 1992, *Bulg. J. Phys.*, **19**, 11.
Brody, T. A., 1993, *The Philosophy Behind Physics*, edited by L. de la Peña and P. E. Hodgson (Berlin: Springer).
Brink, D. M., 1966, Proc. Int. School of Physics, Enrico Fermi, Course XXXVI, Varenna. Ed. C. Bloch (New York, Academic Press).
Brink, D. M. and Boeker, E., 1967, *Nucl. Phys.* **A91**, 1.
Brink, D. M., and Castro, J. J., 1973, *Nucl. Phys.* A, **216**, 109.
Brussaard, P. J., and Glaudemans, P. W. M., 1977, *Shell-Model Applications in Nuclear Spectroscopy* (Amsterdam: North-Holland).
Buck, B., and Merchant, A. C., 1989, *J. Phys.* G, **15**, 615.
Buck, B., Dover, C. B. and Vary, J. P., 1975, *Phys. Rev.* **C11**, 1803.
Buck, B., Merchant, A. C., and Perez, S. M., 1990, *Phys. Rev. Lett.* **65**, 2975.
Buck, B., Merchant, A. C., and Perez, S. M., 1991a, *J. Phys.* **G17**, 1223.
Buck, B., Merchant, A. C., and Perez, S. M., 1991b, *Mod. Phys. Lett.* **A6**, 2453.
Buck, B., Merchant, A. C., and Perez, S. M., 1992, *Phys. Rev.* **C45**, 2247.
Buck, B., Merchant, A. C., Perez, S. M., and Tripe, P., 1994, *J. Phys.* G, **20**, 351.
Byrne, A. P., Dracoulis, G. D., Schiffer, K. J., Davidson, P. M., Kibédi, T., Fabricius, B., Baxter, A. M., and Stuchbery, A. R., 1990, *Phys. Rev.* C, **42**, R6.
Chung, W., van Hienen, J., Wildenthal, B. H. and Bennett, C. L., 1978, *Phys. Lett.* **79B**, 381.
Ciofi degli Atti, C., Pace, E., and Salmé, G., 1989, *Nucl. Phys.* A, **497**, 361c.
Danilin, B. V., Zhukov, M. V., Ershov, S. N., Gareev, F. A., Kurmanov, R. S., Vaagen, J. S., and Bang, J. M., 1991, *Phys. Rev.* C, **43**, 2835.
Dasgupta, M., Walker, P. M., Dracoulis, G. D., Byrne, A. P., Regan, P. H., Kibédi, T., Lane, G. J., and Yeung, K. C., 1994, *Phys. Lett.* B (in press).
Delbar, Th., Grégoire, Gh., Paic, C., Ceuleneer, R., Michel, F., Vanderpoorten, R., Budzanowski, A., Dabrowski, H., Freindl, L., Grotowski, K., Micek, S., Planeta, K., Strzalkowski, A., and Eberhard, K. A., 1978, *Phys. Rev.* **C18**, 1237.
De Shalit, A., and Feshbach, H., 1974, *Theoretical Nuclear Physics I: Nuclear Structure* (New York: Wiley).
Eichler, J., and Faessler, A., 1970, *Nucl. Phys.* A, **157**, 166.
Ferreira, L. S., Maglione, E., Bang, J. M., Thompson, I. J., Danilin, B. V., Zhukov, M. V., and Vaagen, J. S., 1993, *Phys. Lett.* B, **316**, 23.
Fulbright, H. W., Bennett, C. L., Lindgren, R. A., Markham, R. G., McGuire, S. C., Morrison, G. C., Strohbusch, U., and Tōke, J., 1977, *Nucl. Phys.* A, **284**, 329.
Gómez, J. M. G., Prieto, C., and Poves, A., 1992, *Phys. Lett.* B, **295**, 1.
Gottfried, K., 1963, *Ann. Phys. (N.Y.)*, **21**, 29.
Hodgson, P. E., 1963, *The Optical Model of Elastic Scattering* (Oxford University Press).
Hodgson, P. E., 1971, *Nuclear Reactions and Nuclear Structure* (Oxford University Press).
Hodgson, P. E., 1987, *Contemp. Phys.*, **28**, 365.
Hodgson, P. E., 1990, *Contemp. Phys.*, **31**, 295.
Hodgson, P. E., 1992, *Proceedings of the International Conference on Nuclear Data for Science and Technology*, Julich, p. 768.
Hodgson, P. E., 1994, *The Nucleon Optical Potential* (Singapore: World Scientific).
Horiuchi, H. 1985, *Prog. Theor. Phys.* **73**, 1172.
Katō K. and Bandō, H. 1978, *Prog. Theor. Phys.* **59**, 774.
Kobayashi, T., Shimoura, S., Tanihata, I., Katori, K., Matsuta, K., Minamisono, T., Sugimoto, K., Müller, W., Olson, D. L., Symons, T. J. M., and Wieman, H., *Phys. Lett.* B, **232**, 51.
Kobayashi, T., Yamakawa, O., Omata, K., Sugimoto, K., Shimoda, T., Takahasthi, N., and Tanihata, I., 1988, *Phys. Rev. Lett.*, **60**, 2599.
Landau, L. D., and Lifshitz, E. M., 1962, *Quantum Mechanics* (Oxford University Press).
Lawson, R. D., 1980, *Theory of the Nuclear Shell Model* (Oxford University Press).

Leech, J., 1957, *Math. Gaz.*, **41**, 81.
Malaguti, F., Ugnzzoni, A., Verondini, E., and Hodgson, P. E., 1982, *Revista Nuovo Cim.*, **5**, 1.
Marsh, S., and Rae, W. D. M., 1986, *Phys. Lett.*, **B180**, 185.
Mayer, M. G., and Jensen, J. H. D., 1955, *Elementary Theory of Nuclear Shell Structure* (New York: Wiley).
Merchant, A. C., and Buck, B., 1989, *Europhys. Lett.*, **8**, 409.
Merchant, A. C., Pál, K. F., and Hodgson, P. E., 1989, *J. Phys.* G, **15**, 601.
Merchant, A. C., and Rae, W. D. M., 1992, *Nucl. Phys.* **A549**, 431.
Merchant, A. C., and Rae, W. D. M., 1994, *Nucl. Phys.* **A571**, 431.
Michel, F., Reidemeister, G. and Ohkubo, S., 1986a, *Phys. Rev. Lett.* **57**, 1215.
Michel, F., Reidemeister, G. and Ohkubo, S., 1986b, *Phys. Rev.* **C34**, 1248.
Michel, F., Reidemeister, G. and Ohkubo, S., 1988, *Phys. Rev.* **C37**, 292.
Negele, J. W., 1970, *Phys. Rev.* C, **1**, 1260.
Ohkubo, S., 1988, *Phys. Rev.* **C38**, 2377.
Panos, C. N., and Anagnostatos, G. S., 1982, *J. Phys.* G, **8**, 1651.
Price, P. B., 1989, *An. Rev. Nucl. Particle Sci.*, **39**, 19.
Rae, W. D. M., 1988, *J. Phys. Soc. Japan (Suppl.)*, **58**, 77.
Rae, W. D. M., and Merchant, A. C., 1993, Institute of Physics Conference, Glasgow.
Rae, W. D. M., Merchant, A. C., and Buck, B., 1992, *Phys. Rev. Lett.*, **69**, 3709.
Ray, L., and Hodgson, P. E., 1979, *Phys. Rev.* C, **20**, 2403.
Richter, W. A., Van der Merwe, M. G., Julies, R. E., and Brown, B. A., 1991, *Nucl. Phys.* A, **523**, 325.
Rose, H. J., and Jones, G. A., 1984, *Nature*, **307**, 245.
Simmons, P. M., Rae, W. D. M., Davinson, T., Fox, S., Gyapong, G. J., Jones, C. D., Watson, D. L., Clarke, N. M., Fulton, B. R., Leddy, M., Murgatroyd, J. T., Murphy, A., Pople, J., Catford, W. N., and Lilley, J., 1993, Institute of Physics Conference, Glasgow.
Talmi, I., 1984, *Nucl. Phys.*, **A423**, 189.
Talmi, I., 1993, *Simple Theories of Complex Nuclei* (Switzerland: Harwood).
Tanihata, I., 1988, *Nucl. Phys.* A, **488**, 113c.
Thompson, I. J., Al-Khalili, J. S., Tostevin, J. A., and Bang, J. M., 1993, *Phys. Rev.* C, **47**, R1364.
Thompson, I. J., Zhukov, M. V., Danilin, B. V., Fedorov, D. V., Bang, J. M., and Vaagen, J. S., 1993, *Contribution to the Third International Conference on Radioactive Beams*, Michigan, University of Surrey Preprint, No. CNP-93/7.
Tohsaki-Suzuki, A., 1989, *Prog. Theor. Phys., Kyoto*, **81**, 370.
Twin, P. J., Nolan, P. J., Aryaeinejad, R., Love, D. J. G., Nelson, A. H., and Kirwan, A., 1983, *Nucl. Phys.* A, **409**, 343c.
Twin, P. J., Nyakó, B. M., Nelson, A. H., Simpson, J., Bentley, M. A., Cranmer-Gordon, H., Forsyth, P. D., Howe, D., Mokhtar, A. R., Morrison, J. D., Sharpey-Schafer, J. F., and Slettin, G., 1986, *Phys. Rev. Lett.*, **57**, 811.
Varga, K., Lovas, R. G., and Liotta, R. J., 1992a, *Phys. Rev. Lett.*, **69**, 37.
Varga, K., Lovas, R. G., and Liotta, R. J., 1992b, *Nucl. Phys.* A, **550**, 421.
Wada, T. and Horiuchi, H., 1988, *Phys. Rev.* **C38**, 2063.
Walker, P., and Dracoulis, G., 1994, *Phys. World*, **7**, 39.
Wilson, D., 1983, *Rutherford: Simple Genius* (London: Hodder and Stoughton), p. 579.
Wuosmaa, A. H., Betts, R. R., Back, B. B., Freer, M., Glagola, B. G., Happ, Th., Henderson, D. J., Wilt, P., and Bearden, I. G., 1992, *Phys. Rev. Lett.*, **68**, 1295.
Yamaya, T., Oh-ami, S., Fujiwara, M., Itahashi, T., Katori, K., Tosaki, M., Kato, S., Hatori, S., and Ohkubo, S., 1990, *Phys. Rev.* C, **42**, 1935.
Yamaya, T., Ohkubo, S., Okabe, S., and Fujiwara, M., 1993, *Phys. Rev.* **C47**, 2389.
Zamick, L. and Zheng, D. C., 1994, *Z. Phys.* **A349**, 255.
Zhukov, M. V., Danilin, B. V., Fedorov, D. V., Bang, J. M., Thompson, I. J., and Vaagen, J. S., 1993, *Phys. Rep.*, **231**, 151.
Zhukov, M. V., Chulkov, L. V., Fedorov, D. V., Danilin, B. V., Bang, J. M., Vaagen, J. S., and Thompson, I. J., 1994, *J. Phys.* G, **20**, 201.